The Electronic Structure of $[Fe_4S_4]^{3+}$ Clusters in Proteins. An Investigation of the Oxidized High-Potential Iron–Sulfur Protein II from *Ectothiorhodospira vacuolata*†

Lucia Banci,‡ Ivano Bertini,*,‡ Stefano Ciurli,§ Silvia Ferretti,§ Claudio Luchinat,§ and Mario Piccioli‡

Department of Chemistry, University of Florence, Via G. Capponi, 7, 50121 Florence, Italy, and Institute of Agricultural Chemistry, University of Bologna, Viale Berti Pichat, 10, 40127 Bologna, Italy

Received February 23, 1993; Revised Manuscript Received May 25, 1993

ABSTRACT: Within the framework of an investigation of the electronic structure of oxidized high-potential iron–sulfur proteins (HiPIP), we have studied the HiPIP II from *Ectothiorhodospira vacuolata*, which was known to have a peculiar temperature dependence of the ^{1}H NMR isotropic hyperfine shifts. The signals of the cysteine ligand protons have been sequence specifically assigned through NOE, NOESY, and TOCSY experiments. Nine hyperfine-shifted signals are observed: seven in the downfield and two in the upfield region. They have been assigned to the eight β-CH_2 protons of the four coordinated cysteines and to one α-CH cysteine proton. The two most downfield-shifted signals belong to the β-CH_2 protons of Cys 63 (*Chromatium vinosum* numbering) and the two upfield protons to those of Cys 43. These two pairs of protons show a Curie-type temperature dependence of the hyperfine shifts. Among the remaining five downfield-shifted signals, three show a Curie-type temperature dependence and two have an anti-Curie temperature dependence. The former are assigned to the β-CH_2 and α-CH protons of Cys 77 and the latter to the β-CH_2 protons of Cys 46. The shift patterns are thus similar, in a sequence-specific sense, to those of the analogous proteins from *C. vinosum* and *Rhodocyclus gelatinosus*, whereas they differ from those of *Rhodocyclus globiformis* HiPIP and even more from those of *Ectothiorhodospira halophila* HiPIP II. Oxidized HiPIPs can be formally viewed as containing a cluster of four ferric ions plus one extra electron. We present here a model based on a chemical equilibrium, fast on the NMR time scale, between two species, both of which contain a pair of iron(III) ions and a mixed-valence pair but are differently oriented within the protein frame. The EPR data are also discussed in the light of the debate on the nature of the different species detected at low temperature. The interpretation of the whole set of data on HiPIPs in the light of the present model is compared with that based on previous models.

Oxidized high-potential iron–sulfur proteins (HiPIP) contain the $[Fe_4S_4]^{3+}$ polymetal center, which can be formally viewed as containing four Fe^{3+} ions plus one extra electron (Berg & Holm, 1982; Thauer & Schoenheit, 1982; Thompson, 1985). Mössbauer investigations at 4 K point toward an electronic structure of the cluster that can be described as constituted by two Fe^{3+} ions and a mixed-valence pair over which the extra electron is delocalized, giving two $Fe^{2,5+}$ ions (Dickson et al., 1974; Middleton et al., 1980; Bertini et al., 1993a). In this frame work, the total cluster spin $S = {}^1/_2$ can be viewed as given by antiferromagnetic coupling between the S_{12} and S_{34} substrates of the two pairs (Figure 1). Theoretical investigations (Blondin & Girerd, 1990; Munck et al., 1988; Blondin et al., 1992) and ENDOR on model complexes (Rius & Lamotte, 1989; Mouesca et al., 1991) are consistent with a resulting $S_{12} = 4$ or 3 for the ferric pair and $S_{34} = {}^9/_2$ or ${}^7/_2$ for the mixed-valence pair (Rius & Lamotte, 1989; Mouesca et al., 1991; Noodleman, 1988; Banci et al., 1991a; Bertini et al., 1991). In every case, Mössbauer data show that S_{34} is larger than S_{12} (Figure 1) (Dickson et al., 1974; Middleton et al., 1980; Bertini et al., 1993a). ^{1}H NMR data at room temperature have been explained on these bases (Bertini et al., 1991; Banci et al., 1990, 1991b).

The oxidized HiPIP II from *Ectothiorhodospira halophila* shows four β-CH_2 ^{1}H NMR signals of coordinated cysteines

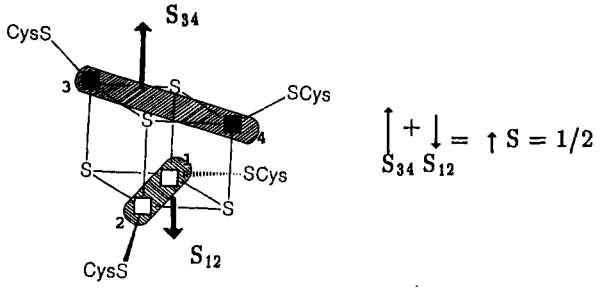

FIGURE 1: Schematic representation of the $[Fe_4S_4]^{3+}$ cluster. The total spin $S = 1/2$ can be viewed as given by antiferromagnetic coupling between the mixed-valence S_{34} pair (■) and the ferric S_{12} pair (□), where $S_{34} = S_{12} + {}^1/_2$ (Dickson et al., 1974; Middleton et al., 1980; Bertini et al., 1993a; Blondin & Girerd, 1990; Münck et al., 1988; Blondin et al., 1992; Rius & Lamotte, 1989; Mouesca et al., 1991; Noodleman, 1988). Possible $|S_{34},S_{12},S\rangle$ ground states are $|{}^9/_2,4,{}^1/_2\rangle$ and $|{}^7/_2,3,{}^1/_2\rangle$ (Rius & Lamotte, 1989; Mouesca et al., 1991).

downfield and four upfield (Krishnamoorthi et al., 1986; Banci et al., 1991c). The former are due to the cysteines bound to the mixed-valence pair, and the latter are due to the cysteines bound to the Fe^{3+} ions (Banci et al., 1991c). The antiferromagnetic coupling between S_{12} and S_{34} is such that, in a magnetic field, the smaller S_{12} in the ground state is oriented in a reversed way with respect to the larger S_{34}, which is quantized along the field, thus providing opposite hyperfine shifts of the nuclei sensing the two sets of iron ions (Noodleman, 1988; Banci et al., 1990, 1991c,d) (Figure 2A). The theoretical treatment does not include spin–orbit coupling nor zero-field

† This work was supported by CNR, Progetto Finalizzato Biotecnologie e Biostrumentazione.

‡ University of Florence.
§ University of Bologna.

0006-2960/93/0432-9387$04.00/0

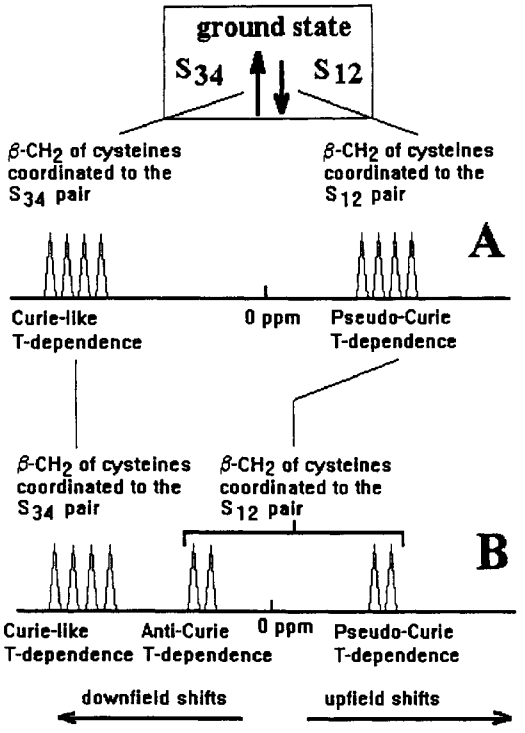

FIGURE 2: Schematic representation of the ^1H NMR spectra of oxidized HiPIPs. In *E. halophila* HiPIP II (A), the β-CH_2 proton signals of the cysteines coordinated to the mixed-valence S_{34} pair are shifted downfield, whereas those of the cysteines coordinated to the ferric S_{12} pair are shifted upfield (Banci et al., 1991). In other oxidized HIPIPs (B) (e.g., *R. gelatinosus*, *C. vinosum*, and *R. globiformis*), one of the two cysteines coordinated to the ferric ions experiences downfield shifts but with an anti-Curie temperature dependence (Bertini et al., 1991, 1992b,c; Nettesheim et al., 1992; Cowan & Sola, 1990).

splitting and considers only one $S = 2$ spin function for the Fe^{2+} ion in tetrahedral geometry. The resulting picture is rather naive, but it provides deep insights. The temperature dependence of the hyperfine shifts is such that the shifts decrease in absolute value with increasing temperature. This, in a way, is what is expected on the basis of the simple Curie law for magnetic susceptibility (Bertini & Luchinat, 1986). Of course, due to the complexity of the system, the extrapolated shifts at infinite temperature are significantly different from the diamagnetic values. However, the upfield shifts extrapolate very far downfield; therefore, we term this behavior pseudo-Curie, and we term the behavior of the downfield signals Curie-like (Figure 2A).

In the case of the oxidized HiPIPs from *Chromatium vinosum* (Bertini et al., 1991; Nettesheim et al., 1983; Cowan & Sola, 1990), *Rhodocyclus globiformis* (Bertini et al., 1993b), and *Rhodocyclus gelatinosus* (Banci et al., 1991b; Nettesheim et al., 1983; Bertini et al., 1992b), one of the two cysteines bound to the Fe^{3+} ions shows ^1H NMR signals slightly downfield. While the other three pairs (two downfield and one upfield) display increasing shifts with decreasing temperature (Curie-like and pseudo-Curie behavior, respectively), the reverse holds for the fourth, slightly downfield pair of protons. Such behavior is termed anti-Curie (Figure 2B). The whole set of data for the latter HiPIPs has been qualitatively accounted for on the basis of pictures involving an overall electronic structure that is less symmetrical than that of *E. halophila* HiPIP II (Figure 3): one in which one iron(III) (for example, iron 1 in Figure 3A) is least involved in the antiferromagnetic coupling within the Fe_4S_4 cluster, and another in which one iron(III) (for example, iron 1 in

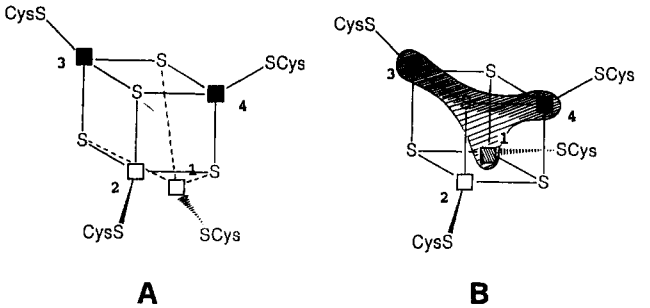

FIGURE 3: Possible low-symmetry situations in the $[Fe_4S_4]^{3+}$ clusters in HiPIPs (mixed-valence iron ions are represented by ■). Iron 1 experiences weaker antiferromagnetic coupling with the other ions (A) or may partially share the extra electron from the mixed-valence pair (B) (Banci et al., 1991b).

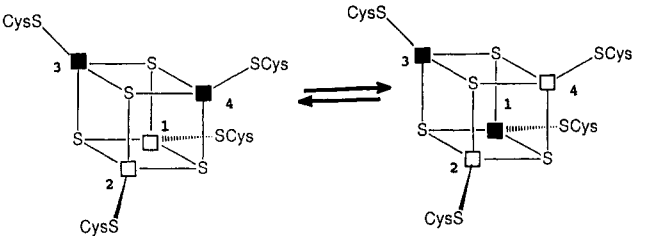

FIGURE 4: Low-symmetry situation obtained in the presence of chemical equilibrium between two situations of higher symmetry. The species on the left has the mixed-valence pair on iron ions 3 and 4, whereas that on the right has the mixed-valence pair on iron ions 3 and 1. As a result, iron 3 is $Fe^{2.5+}$ and iron 2 is Fe^{3+}, whereas iron ions 1 and 4 have oxidation numbers intermediate between 2.5+ and 3+.

Figure 3B) has a noncomplete ferric character (Banci et al., 1991b). In the latter case, this would be the result of partial electronic delocalization from the mixed-valence pair to this ion. Another possibility is the occurrence of a chemical equilibrium between two species, in which one Fe^{3+} and one mixed-valence iron have exchanged their positions within the cluster. The case of chemical equilibrium is illustrated in Figure 4, where the mixed-valence ions and the ferric ions are indicated. We will now explore the consistency of the available data with this possibility.

The progress in NMR spectroscopy of paramagnetic molecules (Lecomte et al., 1991; de Ropp & La Mar, 1991; Bertini et al., 1992c; Banci et al., 1991e; Holz et al., 1992) has led to the sequence-specific assignments of the cysteines bound to the various iron ions (Bertini et al., 1992a,b, 1993b; Nettesheim et al., 1992; Banci et al., 1993). Molecular dynamics (MD) calculations developed by us (Banci et al., 1992a) have proven to be helpful in the absence of an X-ray structure and in providing structural models consistent with the NMR connectivities (Banci et al., 1992a, 1993). The structures around the cluster have been found to be closely related to one another for the systems investigated, and the valence distribution over the iron ions has been compared among the proteins. It appears that *E. halophila* (Banci et al., 1993) and *R. globiformis* (Bertini et al., 1993b) have the same valence distribution, i.e., the mixed-valence pair is bound to Cys 63 and Cys 46 (*C. vinosum* numbering) and the Fe^{3+} ions are bound to Cys 43 and Cys 77. In *R. globiformis*, the iron which is not completely Fe^{3+} (iron 1 in Figures 3 and 4) is bound to Cys 77. In *C. vinosum* (Nettesheim et al., 1992; Bertini et al., 1992a) and *R. gelatinosus* (Bertini et al., 1992b), the mixed-valence pair is bound to Cys 63 and Cys 77, and the Fe^{3+} ions are bound to Cys 43 and Cys 46. The iron which is not completely Fe^{3+} (again, iron 1 in Figures 3 and 4) is bound to Cys 46.

With this in mind, we wanted to investigate an additional HiPIP from a different microorganism. The aim was that of extending the identification of the individual oxidation state of each iron ion of the cluster to more cases, with the hope of obtaining further information on the origin of the inequivalence between the two iron(III) ions. We have chosen the HiPIP II from *Ectothiorhodospira vacuolata*, for which the 1D NMR spectra at 200 MHz were reported in 1986 (Krishnamoorthi et al., 1986). The hyperfine-shifted signals in the oxidized form seemed to experience a nontrivial temperature dependence, which remained unexplained (Krishnamoorthi et al., 1986). In the present article, we confirm the previous observation, correct a misassignment due to lower spectrometer resolution, offer an explanation in terms of the chemical equilibrium between two species, and estimate the difference in energy between them. Finally, we perform the sequence-specific assignment of the cysteine protons by finding specific connectivities between cysteine β-CH_2 protons and the protein frame and by analogy with the ^1H NMR spectra of other HiPIPs.

As a result, we propose that all HiPIPs are better described by the presence of two species: one having the extra electron on the same iron pair as found in *E. halophila* HiPIP II and the other having the extra electron where it is predominantly found in *C. vinosum*, in *R. gelatinosus* HiPIPs, and in the present HiPIP (Figure 4). Equilibria do exist, fast on the NMR time scale, within a cluster between the two electronic distributions described above. The difference in energy between the two states is small or comparable with respect to kT.

EXPERIMENTAL PROCEDURES

Protein Preparation. All chemicals used were of the best quality available. Oxidized HiPIP II was isolated from *E. vacuolata* following the procedure reported for *Ectothiorhodospira shaposhnikovii* (Kusche & Truper, 1984). Protein purity was checked through UV–vis spectroscopy. Sample deuteriation was performed by solvent exchange utilizing an ultrafiltration Amicon cell, equipped with an YM1 membrane. At least five changes of deuteriated buffer were performed to ensure satisfactory solvent exchange.

NMR Measurements. All NMR data have been collected over samples dissolved in 30 mM sodium phosphate buffer at pH 6.1. Protein concentrations were 3–6 mM. All of the NMR spectra were collected on an AMX 600 Bruker NMR spectrometer, operating at the proton Larmor frequency of 600.14 MHz. The temperature was controlled by a Eurotherm variable-temperature control unit. All NMR spectra were calibrated, assigning to the water signal a shift of 4.80 ppm from DSS, at 298 K. The temperature dependence of the water signal was measured independently and used for calibrating the NMR spectra at different temperatures.

NOESY (Macura & Ernst, 1980), COSY (Bax et al., 1981), and TOCSY (Bax & Davis, 1985) experiments in H_2O and D_2O have been performed at temperatures ranging from 280 to 299 K. Mixing times from 10 to 130 ms have been used to follow the buildup of dipolar connectivities. Spin-locking periods from 30 to 80 ms have been used for the TOCSY experiments. The MLEV-17 pulse sequence was used to spin-lock the magnetization in the xy plane of the rotating frame of reference (Bax & Davis, 1985). A complete series of experiments to detect both scalar and dipolar connectivities has been performed in H_2O and D_2O at two different temperatures. 1D NOE experiments have been obtained using the previously reported methodology (Johnson et al., 1983; Banci et al., 1989).

Typically, all of the 2D experiments in the diamagnetic spectral range have been performed by acquiring matrices of 2048 × 750 data points, zero-filled to 2048 × 1024 or 2048 × 2048 data points. Squared-sine or $\pi/2$-shifted squared-sine weighting functions have been applied in both dimensions prior to Fourier transformation. NOESY experiments to detect connectivities involving hyperfine-shifted signals have also been recorded. They have been acquired and processed according to previously reported procedures (Bertini et al., 1992a).

T_1 measurements have been performed using the inversion recovery method (Bertini & Luchinat, 1986; Vold et al., 1968).

EPR Measurements. The EPR spectra at 9.55 GHz were collected at 2 K on a Bruker ER 420 EPR spectrometer equipped with an Oxford cryostat. The field calibration was obtained through an NMR Gauss meter. Field modulation was 100 kHz, and the power values used ranged from 5 to 20 dB.

RESULTS

Pairwise Assignment of the Cysteine β-CH_2 Signals. The 300 K ^1H NMR spectrum of the oxidized form of the HiPIP II from *E. vacuolata* is shown in Figure 5A. The spectrum is reminiscent of that of the HiPIP from *C. vinosum* (Nettesheim et al., 1983; Krishnamoorthi et al., 1986; Bertini et al., 1991). ^1H NOESY experiments performed at 290 K over a spectral window of ca. 50 000 Hz, and optimized for the detection of connectivities among fast-relaxing signals (Figure 5B), allow us to perform a straightforward assignment of the β-CH_2 proton pairs of the coordinated cysteines. It appears that signals C, D, and E are dipolarly connected to one another; signal F is dipolarly connected to signal G, and signal I is dipolarly connected to signal H. Signal A is out of the spectral region in the present experimental conditions; nevertheless, a 1D ^1H NOE experiment allows us to observe that A gives a strong NOE with signal B. From their chemical shift values and their temperature dependencies (see below), signals A–D are assigned to the β-CH_2 of cysteines bound to the dominant mixed-valence S_{34} pair, and signals F–I are assigned to those of cysteines bound to the dominant ferric S_{12} pair (Figure 2). Signal E, which is connected to signals C and D as in *C. vinosum* HiPIP, has a much longer T_1 (Table I) and is therefore assigned as the α-CH proton of the cysteine to which signals C and D belong.

The spreading of the two β-CH_2 signals of each pair is due to the different dihedral angles between the Fe–S–C–H planes and has been essentially accounted for in HiPIPs (Bertini et al., 1992a, 1993b).

Temperature Dependence of the ^1H NMR Spectra. The $1/T$ dependence of the shifts of the hyperfine-shifted signals over the temperature range 280–318 K is reported in Figure 6. All signals show a more or less marked deviation from linearity. Such deviations have not been observed in HiPIPs from other sources (Bertini et al., 1991, 1993b; Banci et al., 1991b, 1993; Nettesheim et al., 1983). In particular, signals A–E show a marked upward curvature with increasing $1/T$ while signals F and G, which experience an anti-Curie temperature dependence, and signals H and I, which are upfield shifted, show a marked downward curvature. Such behavior was already observed in a previous investigation at 200 MHz (Krishnamoorthi et al., 1986). The present higher resolution of the spectrometer allowed us to resolve ambiguities left in the assignments due to signal crossings (Krishnamoorthi et al., 1986).

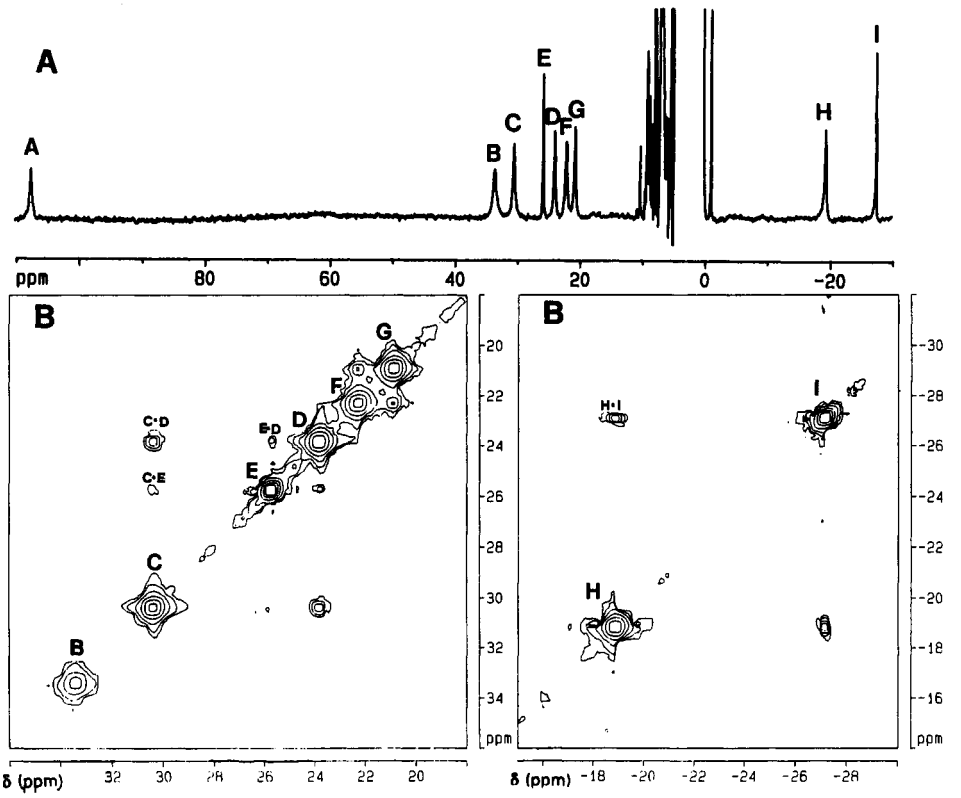

FIGURE 5: (A) 600-MHz (300 K) ^{1}H NMR spectrum of oxidized *E. vacuolata* HiPIP II at pH 6.1. (B) Portions of the 600-MHz ^{1}H NMR NOESY spectrum of oxidized *E. vacuolata* HiPIP II at 290 K, pH 6.1, with a mixing time of 10 ms. The NOESY connectivity between hyperfine-shifted signals (except the cross peak between A and B, observed through 1D NOE) is observed.

Table I: Chemical Shifts and T_1 Values of Hyperfine-Shifted Cysteine Proton Signals of Oxidized HiPIP II from *E. vacuolata* at 300 K and pH 6.3 (*C. vinosum* Numbering)

residue	proton	signal (δ (ppm))	T_1 (ms)[a]
Cys 43	β1	I (-24.7)	43
	β2	H (-13.9)	14
Cys 46	β1	G (22.4)	10
	β2	F (23.7)	9
Cys 63	β1	B (31.9)	4
	β2	A (101.5)	8
Cys 77	β1	D (22.9)	23
	β2	C (29.5)	10
	α	E (25.1)	58

[a] Errors are in the range 10–15%.

Sequence-Specific Assignment of the Cysteine β-CH$_2$ Protons. The primary structure of the present protein is 42% homologous to the primary structure of *C. vinosum* HiPIP (R. P. Ambler, personal communication). Such homology is slightly higher than that found between *C. vinosum* and *R. gelatinosus* (40%) (Przysiecki et al., 1985). In the latter case, the NMR investigation has revealed strict similarities in the tertiary structures and in the location of the amino acid residues around the cluster of the two HiPIPs from different sources (Bertini et al., 1992b). In particular, six of the seven aromatic residues occurring in the primary sequence of *C. vinosum* are conserved in the case of *R. gelatinosus*. On that basis, it was found that the electron distribution within the cluster for *R. gelatinosus* is identical to that found for *C. vinosum* (Bertini et al., 1992a,b). When aromatic residues are considered in the present case, on the basis of unpublished primary sequence data (R. P. Ambler, personal communication), we find that five of the seven aromatic residues occurring in *C. vinosum* are conserved in *E. vacuolata II*. In the case of *C. vinosum*, it has been shown that four aromatic residues (Trp 76, Trp 80, Phe 66, and Tyr 19) are in the proximity of the cluster, and they have been found to be crucial for the assignment of cysteine β-CH$_2$ protons (Bertini et al., 1992a). These residues are all conserved in both *R. gelatinosus* (Przysiecki et al., 1985) and *E. vacuolata* HiPIP II (R. P. Ambler, personal communication). From the X-ray structure of *C. vinosum* (Carter et al., 1974), they are arranged as shown in Figure 7.

The sequence-specific assignment should be straightforward because the regions of the 1D and 2D spectra where the hyperfine-shifted signals fall (Figure 5), as well as the 1D NOEs from the above signal shown as difference spectra in Figure 8, are absolutely similar to those of *C. vinosum* HiPIP. In particular, signals A and B should belong to Cys 63 (*C. vinosum* numbering), signals C–E to Cys 77, signals F and G to Cys 46, and signals H and I to Cys 43. The cysteine signal assignments are reported in Table I, while some of the key assignments used to ensure that the results are univocal are reported in Table II. We give below the essential features of the assignments. The *C. vinosum* numbering will be used throughout. In essence, these assignments are obtained through (1) 1D NOE difference spectra (Figure 8), connecting the nine hyperfine-shifted signals to signals in the diamagnetic region of the spectrum, and (2) identification through NOESY and TOCSY experiments (Figure 9) of the spin patterns and other through-space connectivities in which the latter signals are involved.

The assignment of signal I as Cys 43 Hβ1 is reached by noting that signal I gives three NOEs in the region of the peptide NH protons (signals 1–3 in Figure 8). In the X-ray structure of *C. vinosum*, the Cys 43 Hβ1 is 2.7 Å from Cys 43 NH, 2.9 Å from Ala 44 NH (Leu 44 in *E. vacuolata* HiPIP II), and 2.9 Å from Gly 75 NH. No other cysteine Hβ proton is so close to as many as three NH protons, the next

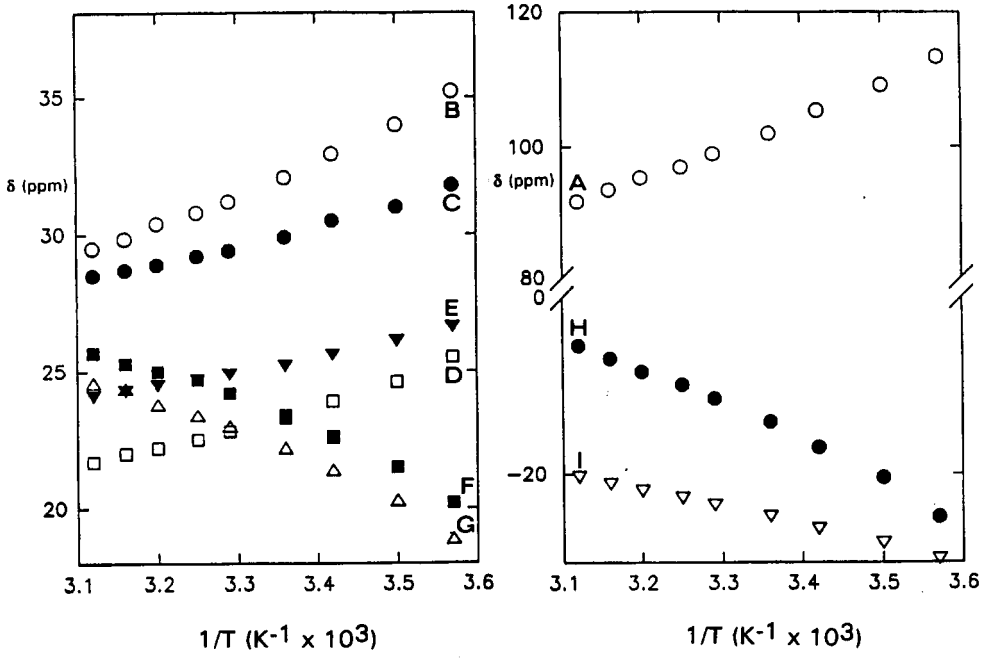

FIGURE 6: Temperature dependence of the chemical shifts of the hyperfine-shifted signals in *E. vacuolata* HiPIP II at pH 6.1.

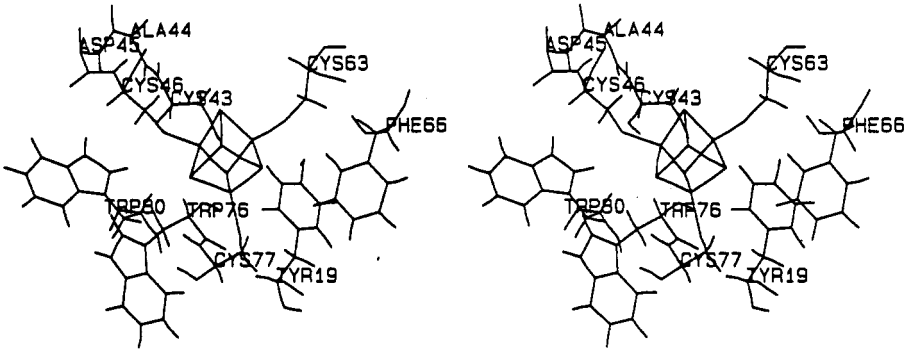

FIGURE 7: Stereoview of the cluster region of oxidized *C. vinosum* HiPIP (Carter et al., 1974). The backbone atoms of residues Leu 44 and Asn 45 are also shown.

Table II: Assignment of the ^{1}H NMR Signals (ppm) of Some Residues in the Proximity of the Cysteine Residues (*C. vinosum* Numbering)

residue	NH	α-CH	β-CH	other
Gly 40	8.70	4.44, 4.11		
Gln 41	7.50	4.18	1.89, 0.20	γ-CH_2: 1.95, 0.29
Thr 42	9.43	6.10	1.70	γ-CH_3: 1.30
Cys 43[a]	9.17		−13.9, −24.7	
Leu 44	7.89	3.38	1.66, 1.57	
Asn 45	7.59	4.54		
Cys 46[a]	7.84	3.40	22.4, 23.7	
Gly 75	8.21	3.84, 3.65		
Trp 76	8.43		4.00, 3.04	NHε: 10.70 Hδ: 7.37 Hζ2: 7.40 Hη: 6.55 Hζ3: 7.02 Hε3: 6.55
Cys 77[a]		25.1	22.9, 29.5	
Trp 80				NHε: 10.22 Hδ: 6.99

[a] See also Table I.

best candidate being Hβ2 of Cys 63, with Phe 66 NH at 2.8 Å, Cys 63 NH at 3.0 Å, and Leu 65 NH at 3.5 Å.

Among the three connectivities from signal I (1–3, Figure 8), the Gly 75 NH should give rise to signal 2 because of the detection of two NH–Hα TOCSY connectivities (4 and 5, Figure 9C) observed at different temperatures. In the NOESY experiments, signals 1 and 3 are connected one another (cross-peak 6, Figure 9A), as expected from the spatial arrangement of the Cys 43 and Leu 44 residues (Figure 7). Further NH(i) – NH(i + 1) connectivities (7 and 8 in Figure 9A) allow the connection of the NH of Leu 44 to that of Asn 45 and the latter to that of Cys 46, again in agreement with structural data (Figure 7). TOCSY connectivities 9 and 10 reveal the Hα protons of Leu 44 and Asn 45 (Table II). The above assignments of the backbone protons of the 43–46 residues are further corroborated by other dipolar connectivities (11–16, see caption to Figure 9).

The NH and Hα of Cys 46 both experience NOEs upon saturation of signals F and G (connectivities 17–20, Figure 8). The latter are therefore assigned as the β-CH_2 protons of Cys 46, with the stereospecific assignment (Table I) relying on the different NOE intensities. All of the other assignments discussed above are summarized in Table II.

The assignment has also been extended from residue 43 back to residue 40 (21–31, see caption to Figure 9), and the side-chain resonances of Gln 41 and Thr 42 have been identified in the TOCSY experiment. The latter residue substitutes (R. P. Ambler, personal communication) for the His 42 present in *C. vinosum* HiPIP (Przysiecki et al., 1985; Carter et al., 1974). The two NOEs from signal G to the exchangeable resonance 32 and to the broad resonance 33 (Figure 8), which are dipolarly connected one another (cross-peak 34, Figure

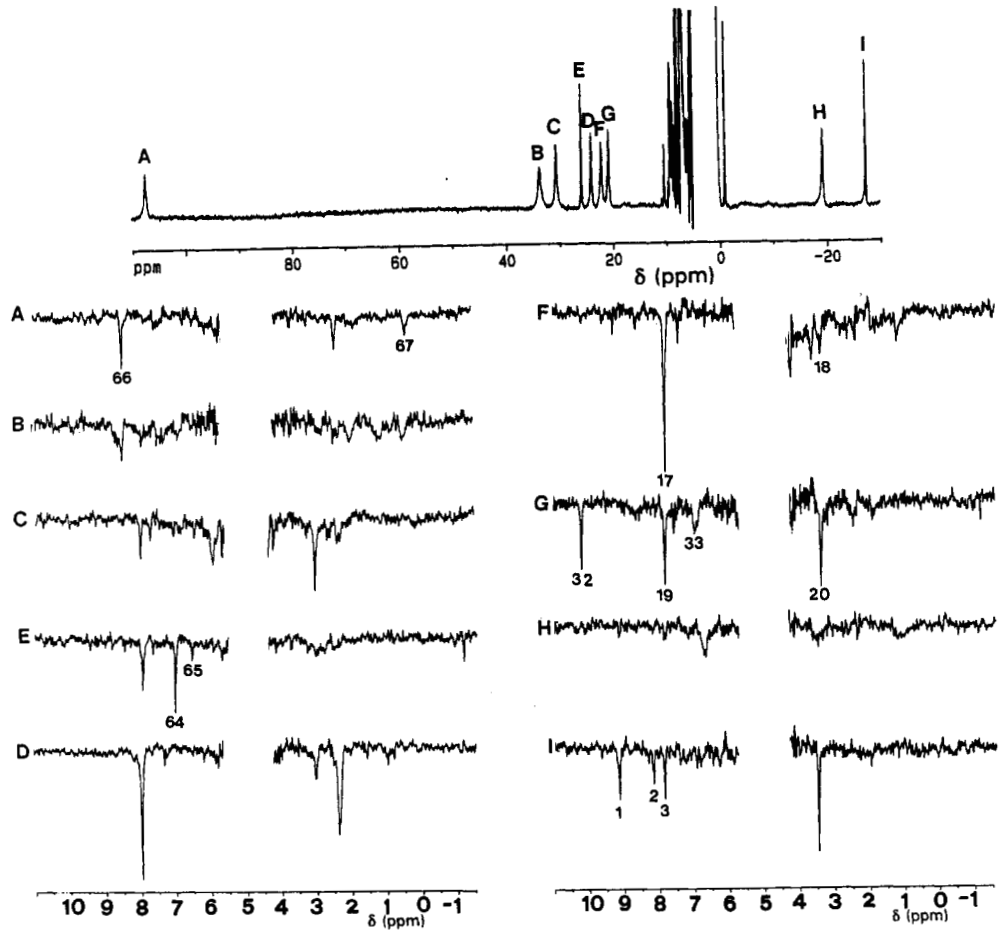

FIGURE 8: 600-MHz (290 K) ^{1}H NOE difference spectra obtained upon saturation of the hyperfine-shifted signals of *E. vacuolata* HiPIP II. The reference spectrum is reported on the top of the figure. Each difference spectrum is labeled according to the saturated signal. The vertical scale of the spectra is calibrated in such a way that the areas of the saturated signals are all equal. Assignments of the NOE peaks indicated with numbers and discussed in the text are as follows: (1) C43 CHβ2–C43 NH, (2) C43 CHβ2–G75 NH, (3) C43 CHβ2–L44 NH, (17) C46 CHβ2–C46 NH, (18) C46 CHβ2–C46 CHα, (19) C46 CHβ1–C46 NH, (20) C46 CHβ1–C46 CHα, (32) C46 CHβ1–W80 NHϵ, (33) C46 CHβ1–W80 CHδ, (64) C77 CHα–W76 CHϵ3, (65) C77 CHα–W76 CHη3, (66) C63 CHβ2–C63 NH, (67) C63 CHβ2–V17 γCH3. The latter two assignments are tentative.

9A), are quite consistent with the presence of the indole ring of Trp 80 at a short distance from one of the geminal protons of Cys 46. Further connectivities are observed between the NH of Trp 80 and signals already assigned (connectivities 35–39; see caption for Figure 9 and Table II).

From the NH resonance of Gly 75, it is possible to identify the peptide NH signal of Trp 76 by the following network of dipolar connectivities (Figure 9B): Gly 75 NH–Gly 75 Hα1 (40), Gly 75 NH–Gly 75 Hα2 (41), Gly 75 Hα1–Trp 76 NH (42), Gly 75 Hα2–Trp 76 NH (43). The Gly 75 NH–Gly 75 Hα connectivities have also been observed in the TOCSY experiment (connectivities 4 and 5, Figure 9C). The Trp 76 Hα and Cys 77 NH signals are not detected, possibly because they are very close to the cluster and are broadened by dipolar relaxation from the paramagnetic center (Banci et al., 1991d); nevertheless, an extended network of dipolar connectivities has been observed (44–59, see cation of Figure 9), as well as a distinguishable TOCSY pattern (60–63, Figure 9C), which allows us to assign all of the Trp 76 resonances except its Hα proton. The whole spin pattern typical of a Trp six-membered ring is not fully apparent in Figure 9C due to the overlap between the Hϵ3 and Hζ3 signals. When the experiment is performed at 299 K, the overlap between the two signals is removed. The 75–77 fragment is conserved in all of the HiPIPs for which the primary sequence has been obtained, except for the HiPIP from *Rhodospirillum tenue* in which Trp 76 is replaced by Tyr (Przysiecki et al., 1985). Therefore, the observed dipolar inter-residue connectivities can be safely interpreted on the basis of homology with the *C. vinosum* structure (Figure 7) (Carter et al., 1974).

The assignment of Trp 76 resonances provides univocal proof for signals C–E to be assigned as Cys 77 resonances (Table I). Signal E gives NOEs (Figure 8) with Trp 76 Hϵ3 (64) and with Trp 76 Hζ3 (65). No Hα cysteine proton but the one belonging to Cys 77 is close in space to protons of the six-membered ring of a Trp residue. Again, this very same spatial arrangement appears in the X-ray structure of *C. vinosum* HiPIP (Carter et al., 1974) and is observed by NMR in *C. vinosum* (Bertini et al., 1992a), *R. gelatinosus* (Bertini et al., 1992b), and *E. halophila* (iso II) (Banci et al., 1993) HiPIPs. Further evidence for the assignment of Cys 77 is provided by the strong NOE observed from signals C–E to a signal at 4.86 ppm. This NOE is not shown in Figure 8 due to the nonsatisfactory quality of the difference spectra in the proximity of the water signal, but it is clearly observed when the experiments are performed in D_2O. Again, the same connectivities were also observed, at the same extent as that found here, for *C. vinosum* (Bertini et al., 1992a), *R. gelatinosus* (Bertini et al., 1992b), and *E. halophila* (Banci et al., 1993) HiPIPs. The signal at 4.86 ppm can be attributed to the Tyr 19 Hα resonance, which is the only proton close to all three protons of Cys 77. The stereospecific assignment

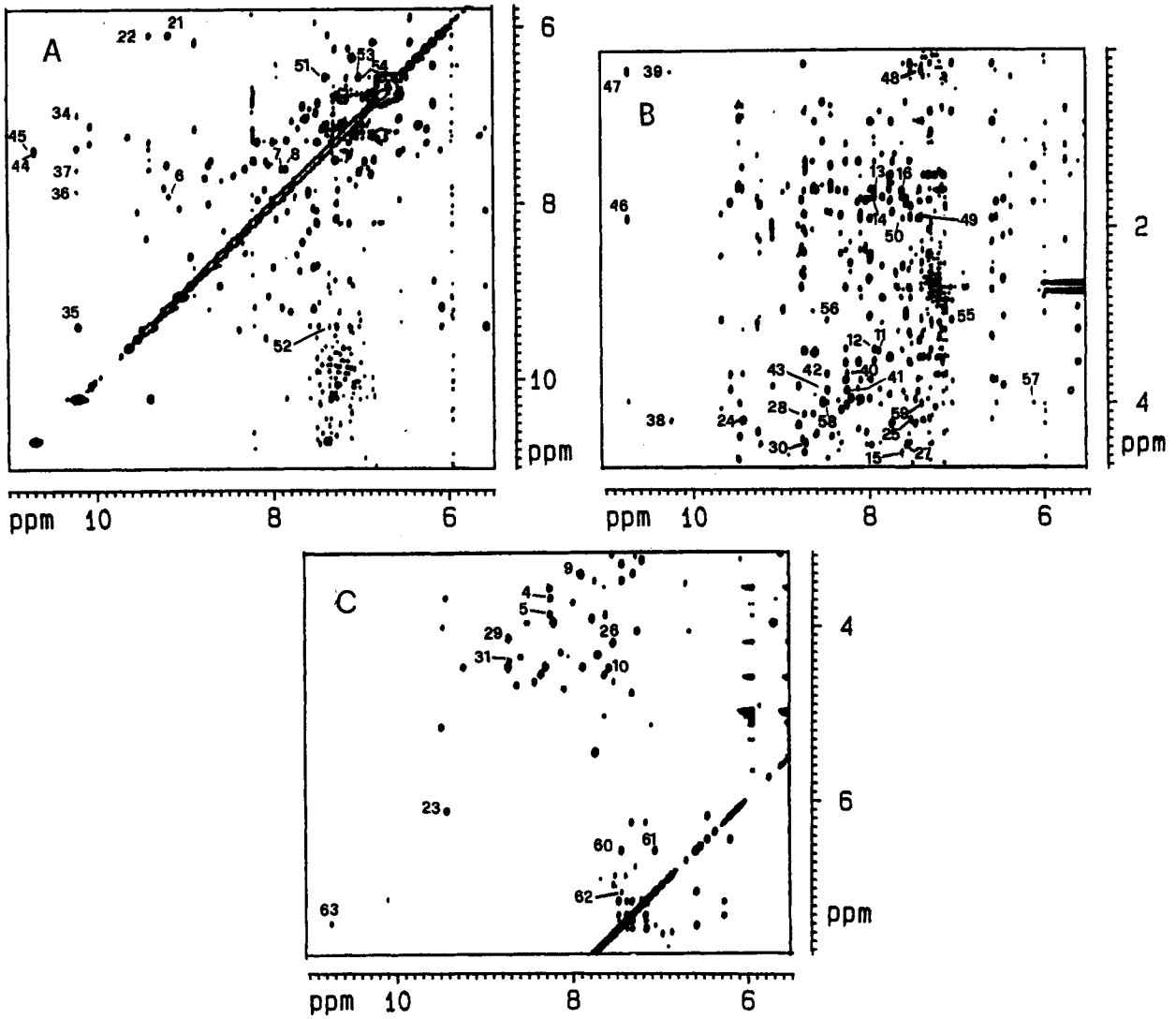

FIGURE 9: 600-MHz ^{1}H NMR NOESY (A and B) and TOCSY (C) spectra recorded in H_2O solutions at 290 K with mixing times (A) and spin-locking times (B) of 30 ms. 2K × 500 data points have been collected and transformed using a 2K × 1K data point matrix. Prior to Fourier transformation, squared-sine functions were applied, shifted by $\pi/3$ in the F2 dimension and by $\pi/4$ in the F1 dimension. We list here the assignments of the cross peaks indicated with numbers in Figure 9 and discussed in the text. NOESY: (6) C43 NH–L44 NH, (7) L44 NH–N45 NH, (8) N45 NH–C46 NH, (11) C46 NH–C46 CHα, (12) L44 NH–L44 CHα, (13) L44 NH–L44 CHβ, (14) L44 NH–L44 CHβ, (15) N45 NH–N45 CHα, (16) N45 NH–L44 CHβ, (21) C43 NH–T42 CHα, (22) T42 CHα–T42 NH, (24) T42 NH–Q41 CHα, (25) Q41 NH–Q41 CHα, (27) Q41 NH–G40 CHα, (28) G40 NH–G40 CHα', (30) G40 NH–G40 CHα, (34) W80 CHϵ–W80 CHδ, (35) W80 NHϵ–T42 NH, (36) W80 NHϵ–C46 NH, (37) W80 NHϵ–N45 NH, (38) W80 NHϵ–Q41 CHα, (39) W80 NHϵ–Q41 CHβ, (40) G75 NH–G75 CHα, (41) G75 NH–G75 CH$'\alpha$, (42) G75 CHα–W76 NH, (43) G75 CHα'–W76 NH, (44) W76 NHϵ–W76 CHζ2, (45) W76 NHϵ–W76 CHδ, (46) W76 NHδ–Q41 CHβ', (47) W76 NHδ–Q41 CHβ, (48) W76 CHδ–Q41 CHβ, (49) W76 CHδ–Q41 CHβ', (50) Q41 CHβ'–Q41 NH, (51) W76 CHζ2–W76 CHη, (52) W76 CHδ–T42 NH, (53) W76 CHη–W76 CHζ3, (54) W76 CHϵ3–W76 CHζ3, (55) W76 CHϵ3–W76 CHβ, (56) W76 NH–W76 CHβ, (57) T42 CHα–W76 CHβ, (58) W76 NH–W76 CHβ', (59) W76 CHδ–W80 CHβ'. TOCSY: (4) G75 NH–G75 CHα, (5) G75 NH–G75 CHα', (9) L44 NH–L44 CHα, (10) N45 NH–N45 CHα, (23) T42 NH–T42 CHα, (26) Q41 NH–Q41 CHα, (29) G40 NH–G40 CHα', (31) G40 NH–G40 CHα, (60) W76 CHζ2–W76 CHη, (61) W76 CHη–W76 CHζ3 and W76 CHϵ3–W76 CHζ3, (62) W76 CHζ2–W76 CHζ3, (63) W76 NHϵ–W76 CHδ.

of signals C and D (Table I) is achieved by using their T_1 values as indicators of their distance from the metal and by the relative intensities of their NOEs to signal E. The assignment of Gly 40–Cys 46 and Gly 75–Cys 77 residues is also summarized in Table II.

Obviously, signals A and B can be assigned to Cys 63 by exclusion (Table I). This assignment is further corroborated by their NOEs (Figure 8). The NOE difference spectrum obtained upon saturation of signal A reveals a strong NOE at 8.44 ppm (66) and an NOE in the region of the methyl resonances at 0.37 ppm (67), which are strongly reminiscent of the connectivities observed from signal A in the case of previously investigated HiPIPs (Banci et al., 1993; Bertini et al., 1992a,b, 1993b) and tentatively assigned to the Cys 63 NH and to a CH_3 group of either a Val or an Ile occurring at position 71, depending on the protein. This residue is close to the cluster and at a very short distance from at least one of the two β-CH_2 protons.

The assignment of cysteine proton resonances is summarized in Table I. The stereospecific assignment of the β-CH_2 protons within each pair is obvious, from the connectivities discussed above, for cysteines 43, 46, and 77. For Cys 63 the assignment is performed by analogy with other HiPIPs, given the strong difference in hyperfine shifts and relaxation rates between the A and B signals. Because our aim is only to demonstrate that the assignment of the hyperfine-shifted signals in *E. vacuolata* HiPIP II is the same as that for *C. vinosum* HiPIP (Bertini et al., 1992a), we will not further discuss the overall set of scalar and dipolar connectivities, and we will not extend the assignment to other parts of the sequence.

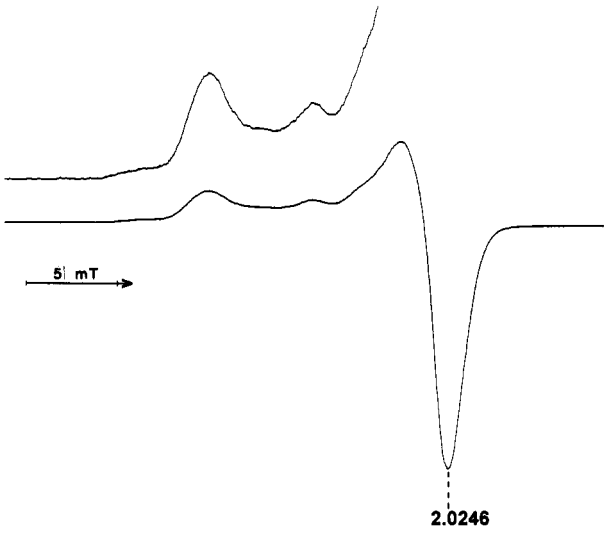

FIGURE 10: X-band (9.55 GHz) EPR spectrum of oxidized HiPIP II from *E. vacuolata* recorded at 2 K. The sample is in 30 mM phosphate buffer, pH 6.3.

We would like to stress again that the assignment at which we arrived through the analysis of all of the cross peaks explained in the text and in the captions to Figures 8 and 9 is exactly that which we would have expected from simply comparing the spectra of the present HiPIP with that from *C. vinosum*. Indeed, in both cases the β-CH_2 protons of Cys 43 are upfield-shifted and have characteristically different line widths, and the temperature dependencies of their hyperfine shifts have characteristically different slopes. In both cases, Cys 77 is unique in that all three signals of the cysteine are outside the diamagnetic region. In both cases, Cys 46 β-CH_2 proton resonances are characterized by anti-Curie behavior. Finally, in both cases Cys 63 β-CH_2 protons are the most downfield-shifted and experience the largest splitting within the pair.

EPR Spectra. The EPR spectrum recorded at low temperature is reported in Figure 10. It shows four features at $g = 2.14, 2.10, 2.07$, and 2.03. This is very closely reminiscent of the spectrum of *C. vinosum* HiPIP (Antanaitis & Moss, 1975; Dunham et al., 1991). Such types of spectra had first been interpreted as due to two main species: one with $g_\parallel$ at about 2.11 and another with $g_\parallel \cong 2.07$ (Antanaitis & Moss, 1975). Recently, the spectrum of *C. vinosum* HiPIP was reinterpreted as due to two species with very similar $g_\parallel$ values corresponding to $g_\parallel \cong 2.11$ (Dunham et al., 1991). The features at $g = 2.13$ and 2.07 have been attributed to a third species whose intensity is below 10%.

DISCUSSION

The sequence-specific assignment shows that the framing of the cluster in the protein from *E. vacuolata* HiPIP II is the same as that of *C. vinosum* HiPIP, but different from that of *E. halophila* HiPIP II. Figure 11 shows the ^{1}H NMR spectra of all of the oxidized HiPIPs for which the assignment is available. A trend is apparent from *E. halophila* HiPIP II (A) (Krishnamoorthi et al., 1986; Banci et al., 1991c, 1993) to *R. globiformis* (B) (Bertini et al., 1993b), to the present *E. vacuolata* HiPIP II (C), to *C. vinosum* (D) (Nettesheim et al., 1983, 1992; Cowan & Sola, 1990; Bertini et al., 1991, 1992a), and to *R. gelatinosus* (E) (Nettesheim et al., 1983; Banci et al., 1991b; Bertini et al., 1992b). The β-CH_2 protons of Cys 77 (signals C and D), which are upfield in *E. halophila* HiPIP II, reflecting the virtually pure ferric character of the corresponding iron ion, move downfield in *R. globiformis*, where they show anti-Curie temperature dependence, and progressively more downfield with Curie-like temperature dependence in the other proteins, indicating their increasing involvement in the mixed-valence pair. In turn, the β-CH_2 protons of Cys 46 (signals F and G) move from essentially belonging to the mixed-valence pair in *E. halophila* HiPIP II (sizably downfield and with Curie-like temperature dependence) to being less downfield and with a strong anti-Curie behavior in *R. gelatinosus*. A protein representing the existence of the opposite extreme to *E. halophila* HiPIP II (i.e., with F and G upfield and pseudo-Curie) has not yet been found.

The spectra with six β-CH_2 signals downfield and two upfield of *C. vinosum* and *R. gelatinosus* HiPIPs had been interpreted by us as evidence of low-symmetry components which would cause inequivalence between the two Fe^{3+} ions as well as between the two partners of the mixed-valence pair (Banci et al., 1991a,b; Bertini et al., 1991). The extra electron—with respect to a cluster containing four Fe^{3+} ions—would be delocalized only on a mixed-valence pair in the symmetric case encountered in *E. halophila* HiPIP II, whereas it would also be partially delocalized on a third iron ion in all of the other nonsymmetric cases (Figure 3B) (Banci et al., 1991b). The inequivalence would somehow be controlled by the protein part of the molecule. The discovery of the existence of two different orientations of the cluster within the protein from (i.e., one orientation with the two Fe^{3+} ions bound to Cys 43 and Cys 77, and the other with the two Fe^{3+} ions bound to Cys 43 and Cys 46) (Bertini et al., 1992a, 1993b; Banci et al., 1993), together with the present data indicating somewhat intermediate behavior, leads us to take into consideration the possibility of a chemical equilibrium between these two species coexisting in the same protein (Figure 4). If the equilibrium is fast on the NMR time scale, and the two species at room temperature are present in comparable amounts, the resulting time-averaged picture is that one iron is Fe^{3+} (iron 2 in Figure 4), another is $Fe^{2.5+}$ (iron 3 in Figure 4), and the other two have intermediate oxidation numbers, one closer to Fe^{3+} and the other closer to $Fe^{2.5+}$, if the ratio between the two species is not 50:50. As expected, the present fast chemical equilibrium picture and the picture based on electron delocalization (Banci et al., 1991b) are very similar, and they are barely distinguishable.

The temperature dependence of the contact shifts has been predicted for the electron delocalization case (Banci et al., 1991b). It can be easily predicted for the chemical equilibrium case, as shown below. In the symmetric case containing only one species, the Hamiltonian for the system can be solved analytically to obtain the wave functions and the energies. The latter are given by the following (Noodleman, 1988; Bertini et al., 1991):

$$E = JS(S+1) + \Delta J_{12}S_{12}(S_{12}+1) + \Delta J_{34}S_{34}(S_{34}+1) \quad (1)$$

where J is the antiferromagnetic coupling constant experienced by all pairs in the cluster but the 1–2 and 3–4 pairs, these experience $J + \Delta J_{12}$ and $J + \Delta J_{34}$ coupling constants, respectively. 1 and 2 refer here to the Fe^{3+} ions and 3 and 4 to the mixed-valence pair.

From the wave functions, the hyperfine coupling constant of each level for each metal ion can be calculated (Noodleman,

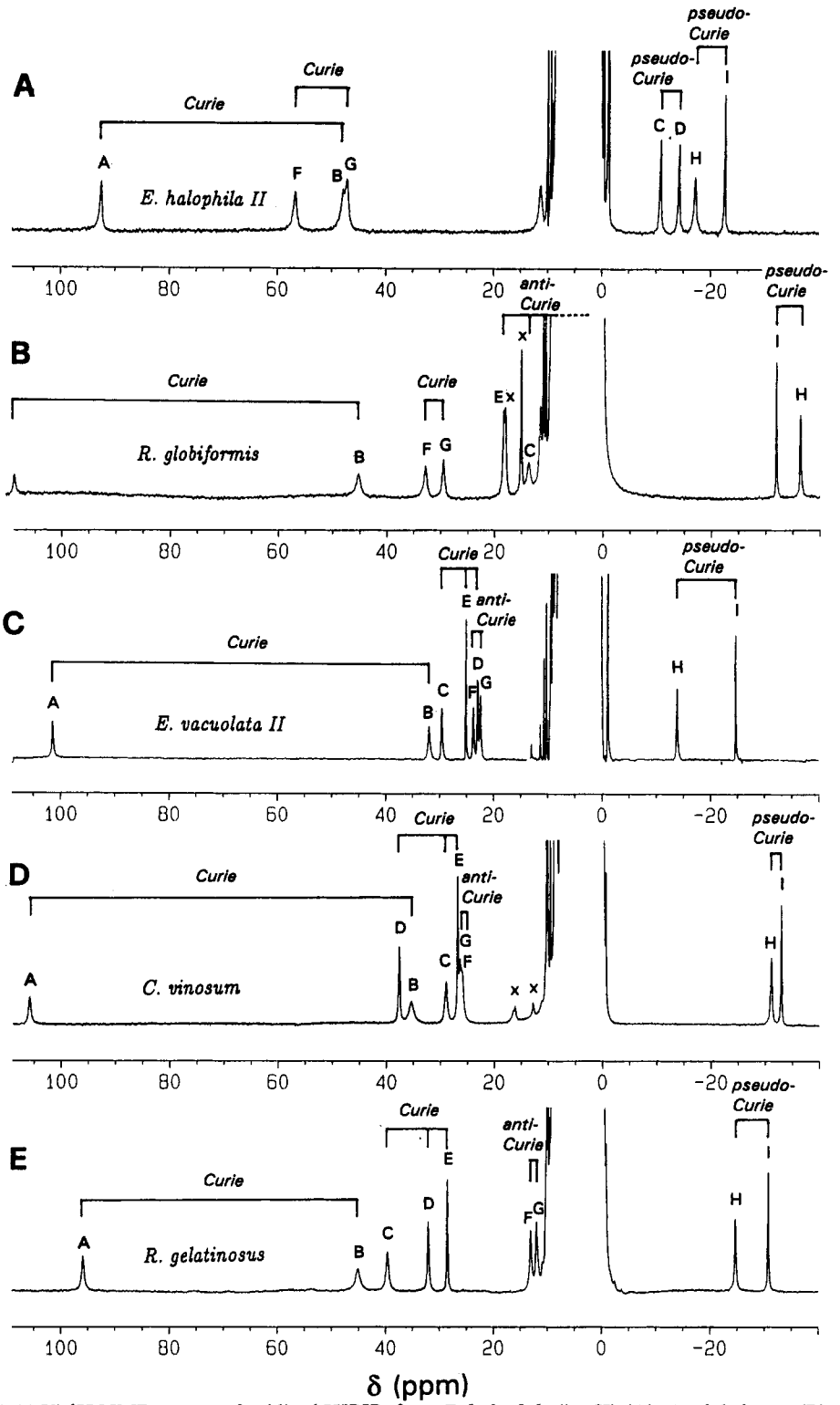

FIGURE 11: 600-MHz (300 K) ^{1}H NMR spectra of oxidized HIPIPs from *E. halophila* (iso-II) (A), *R. globiformis* (B), *E. vacuolata* (iso-II) (C), *C. vinosum* (D), and *R. gelatinosus* (E). For all of the proteins, the eight β-CH_2 signals are labeled according to the sequence-specific assignment of the present protein (Table I, *C. vinosum* numbering). Note that in all but the *E. halophila* (iso-II) case, the α-CH proton of Cys 77 is also apparent (signal E) well outside the diamagnetic spectral region. The Curie, anti-Curie, and pseudo-Curie temperature dependencies are also indicated. Signals labeled with x are residual signals from the reduced protein.

1988), whereas from the energy spacing of the levels, the temperature dependence of the shifts can be evaluated (Bertini et al., 1991; Banci et al., 1990). A typical calculated $1/T$ profile is reported in Figure 12A. Note that the shifts of the mixed-valence pair should be averaged by electron delocalization (Noodleman, 1988). [As pointed out above, introduction of anisotropic components to account for electron delocalization in a third iron removes the degeneracy of the two Fe^{3+} ions and causes the profiles to deviate more sizably from linearity (Banci et al., 1991b).]

In the case of chemical equilibrium, the system is constituted by two species, both of the symmetric type described above. One species has, for instance, the mixed-valence pair on ions 3 and 4, with the energies given by eq 1, whereas the other

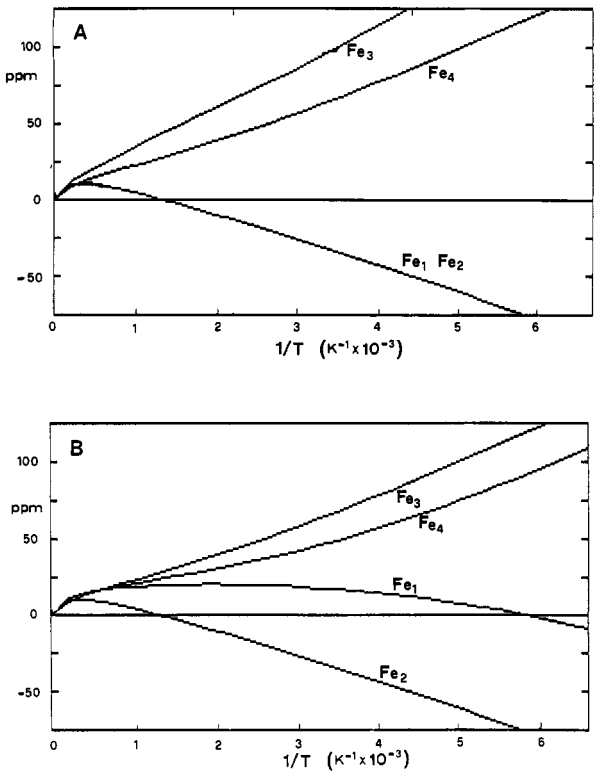

FIGURE 12: Calculated temperature dependence of the ^1H NMR hyperfine shifts of HIPIPs in the absence (A) and in the presence (B) of equilibrium. The parameters in eq 1 are $J = 300$ cm^{-1} and $\Delta J_{12} = -\Delta J_{34} = 100$ cm^{-1}, and those in eq 2 are $J = 300$ cm^{-1} and $\Delta J_{24} = -\Delta J_{13} = 100$ cm^{-1}. $\Delta E = 90$ cm^{-1}, corresponding to ca. 40:60 distribution around room temperature. Fe_3 corresponds to the iron bound to Cys 63, Fe_4 to that bound to Cys 77, Fe_1 to that bound to Cys 46, and Fe_2 to that bound to Cys 43. Fe_3 is always part of the mixed-valence pair, Fe_2 is always ferric, and Fe_4 spends a larger share of time than Fe_1 in the mixed-valence pair.

has the mixed-valence pair on ions 1 and 3 and energies given by

$$E = JS(S+1) + \Delta J_{24}S_{24}(S_{24}+1) + \Delta J_{13}S_{13}(S_{13}+1) \quad (2)$$

Note that eqs 1 and 2 are identical, except for the reversal of labels 1 and 4. These are the two species in equilibrium. We can then make the hypothesis that the ground state of the second species is offset by an energy ΔE with respect to the ground state of the first species to account for different positions of the equilibrium. The calculated temperature dependence of the shifts is then obtained by summing up the contributions from both energy ladders. Under such conditions, the low-temperature limit is the same as that of the single species which lies lower in energy, whereas in the high-temperature limit both ladders are populated equally and the two species contribute 50% each. Figure 12B shows a profile obtained with $J = 300$ cm^{-1}, $\Delta J_{12} = -\Delta J_{34} = 100$ cm^{-1} in eq 1, $\Delta J_{24} = -\Delta J_{13} = 100$ cm^{-1} in eq 2, and $\Delta E = 90$ cm^{-1}. The J and ΔJ values are the same as those used in previous calculations, where $\Delta E = 90$ cm^{-1} has been chosen to give a ca. 40:60 distribution around room temperature.

A peculiarity of the profiles in Figure 12B is a striking deviation from linearity. This deviation is understood in terms of the superposition, to the almost linear temperature dependence of cases 1 and 2 taken separately, of the strong temperature dependence of the equilibrium position between the two, which starts from 50:50 at the left-hand side of the figure and approaches 0:100 toward the right-hand side of the figure. The strong nonlinearity introduced by the presence of the equilibrium is barely obtainable by using the model involving partial delocalization on a third iron ion (Banci et al., 1991b).

Thus, the striking deviation from linearity observed experimentally for most β-CH_2 signals is better reproduced by the equilibrium model. By using larger ΔE values (i.e., by assuming predominance of one of the two species), the curvatures are much reduced, and the experimental profiles of all of the other HiPIPs can be reproduced equally well.

Mössbauer spectra indicate that, in *C. vinosum* (Middleton et al., 1980), only one symmetrical species is present with the same parameters as those in *E. halophila* HiPIP II (Bertini et al., 1993a). The models which do not require equilibrium account for such a spectrum at 4 K because the ground state is quasisymmetric (Banci et al., 1991b). Likewise, the equilibrium model can be consistent either with a single species which is the most thermodynamically stable or, if the two species are frozen out, with the lack of resolution. Indeed, the two clusters depicted in Figure 4 are expected to have very similar Mössbauer parameters. Therefore, Mössbauer data are not expected to discriminate between the two models. For the same reasons, discrimination is not expected from magnetic susceptibility data.

On the other hand, proton ENDOR studies on single crystals of $[Fe_4S_4]^{3+}$ clusters in a model compound show evidence of heterogeneity of the electron distribution very much like the one depicted in Figure 4 (Mouesca et al., 1991; Rius & Lamotte, 1989), indicating that, at least for a symmetric model compound, different electronic distributions may indeed coexist.

The EPR spectra of oxidized HiPIPs could be, in principle, of more help, because freezing of the two species in equilibrium should result in the superposition of their EPR spectra, not necessarily indistinguishable. EPR spectra have been reported for the oxidized forms of *C. vinosum* (Dunham et al., 1991; Antanaitis & Moss, 1975), *E. halophila* (Bertini et al., 1993a), and *R. gelatinosus* (Beinert & Thomson, 1983), besides the present protein. Unfortunately, their interpretation is not straightforward. Only the EPR spectrum of *E. halophila*, which in our opinion contains one symmetric species in any case, is consistent with a single species, $g_\parallel$ being 2.146 and $g_\perp$ being 2.030 (Bertini et al., 1993a). In the case of *C. vinosum*, it has been suggested that there are two dominant species, one being monomeric and the other dimeric, with very similar EPR parameters (Dunham et al., 1991). The spectrum of the *R. gelatinosus* protein is of the same type (Beinert & Thomson, 1983). It would be tempting to assign these two species to the two species which are in equilibrium at 300 K, but frozen out at 2 K. Interestingly, the EPR spectra of the present oxidized HiPIP also show the same kind of heterogeneity observed for *C. vinosum* and *R. gelatinosus* HiPIP. In this respect, the EPR data are consistent with our model. However, we believe that, in the absence of further experimental data of the type of single-crystal EPR or ENDOR, it is impossible to fully assign each low-temperature EPR feature to a well-defined species.

A brief comment on the possible time scale of the proposed equilibrium is due. The room-temperature NMR data can be used to estimate a lower limit of 10^5 s^{-1} for the exchange rate. Since the proposed electronic rearrangement is relatively modest, it is likely to imply only small atomic displacements, and therefore, rates faster than 10^5 s^{-1} are perfectly plausible. On the other extreme, Mössbauer (and possibly EPR) data

show that the equilibrium is frozen at low temperatures on the respective time scales.

CONCLUSIONS

We have shown that, among the six HiPIPs investigated up to now through ^1H NMR, only one (the HiPIP II from *E. halophila*) can be described by two essentially equivalent iron(III) ions and a mixed-valence pair. All of the other HiPIPs deviate from this model. A low-symmetry model (Banci et al., 1991b) is capable of explaining all of the essential spectroscopic features, but leaves each system with different extents and different locations of asymmetry.

Alternatively, an equilibrium between two species differing for the pair of iron ions involved in valence mixing is also nicely consistent with the experimental data. Even the peculiar temperature dependences of the shifts are easily reproduced. The low-symmetry component model tends to make one iron(III) nonequivalent from the other, and only a particular distortion of the cluster makes the two mixed-valence irons inequivalent. The present model makes one iron(III) nonequivalent from the other as much as one mixed-valence iron from the other. Figure 11 is qualitatively consistent with the latter model.

Resonance Raman studies have shown a number of vibrational Fe–S stretching modes larger than expected (Backes et al., 1991). The authors wonder that NMR gives no indication of multiple conformers. Indeed, this could be a matter of time scale, as the equilibrium between species is fast on the NMR time scale and slow on the resonance Raman time scale. The position of the equilibrium would be determined by the electric field caused by the charges of the protein atoms and by the metal ligands. Such a model is quite attractive and satisfies chemical intuition, according to which the addition of one electron to one Fe_4S_4 cluster containing all Fe^{3+} ions may well not be univocal, i.e., it may result in more than one energy minimum.

ACKNOWLEDGMENT

We are grateful to Prof. Jürgen Hütterman for access to the EPR spectrometer and for competent assistance in collecting the EPR spectra. Thanks are expressed to Dr. R. P. Ambler for making the primary sequence data of *E. vacuolata* HiPIP II available to us.

REFERENCES

Antanaitis, B. C., & Moss, T. H. (1975) *Biochim. Biophys. Acta 405*, 262.

Backes, G., Mino, Y., Loehr, T. M., Meyer, T. E., Cusanovich, M. A., Sweeney, W. V., Adman, E. T., & Sanders-Loehr, J. (1991) *J. Am. Chem. Soc. 113*, 2055–2064.

Banci, L., Bertini, I., Luchinat, C., Piccioli, M., Scozzafava, A., & Turano, P. (1989) *Inorg. Chem. 28*, 4650–4656.

Banci, L., Bertini, I., & Luchinat, C. (1990) *Struct. Bonding 72*, 113–135.

Banci, L., Bertini, I., Briganti, F., & Luchinat, C. (1991a) *New J. Chem. 15*, 467–477.

Banci, L., Bertini, I., Briganti, F., Luchinat, C., Scozzafava, A., & Vicens Oliver, M. (1991b) *Inorg. Chem. 30*, 4517–4524.

Banci, L., Bertini, I., Briganti, F., Luchinat, C., Scozzafava, A., & Vicens Oliver, M. (1991c) *Inorg. Chim. Acta 180*, 171–175.

Banci, L., Bertini, I., & Luchinat, C. (1991d) in *Nuclear and Electron Relaxation. The Magnetic Nucleus-Unpaired Electron Coupling in Solution*, VCH, Weinheim, Germany.

Banci, L., Bertini, I., Turano, P., Tien, M., & Kirk, T. K. (1991e) *Proc. Natl. Acad. Sci. U.S.A. 88*, 6956–6960.

Banci, L., Bertini, I., Carloni, P., Luchinat, C., & Orioli, P. L. (1992a) *J. Am. Chem. Soc. 114*, 10683–10689.

Banci, L., Bertini, I., Capozzi, F., Carloni, P., Ciurli, S., Luchinat, C., & Piccioli, M. (1993) *J. Am. Chem. Soc. 115*, 3431–3440.

Bax, A., & Davis, D. G. (1985) *J. Magn. Reson. 65*, 355–360.

Bax, A., Freeman, R., & Morris, G. (1981) *J. Magn. Reson. 42*, 164–168.

Beinert, H., & Thomson, A. J. (1983) *Arch. Biochem. Biophys. 222*, 333.

Berg, J. M., & Holm, R. H. (1982) in *Iron–Sulfur Proteins* (Spiro, T. G., Ed.) pp 1–66, Wiley-Interscience, New York.

Bertini, I., & Luchinat, C. (1986) in *NMR of Paramagnetic Molecules in Biological Systems*, Benjamin/Cummings, Menlo Park, CA.

Bertini, I., Briganti, F., Luchinat, C., Scozzafava, A., & Sola, M. (1991) *J. Am. Chem. Soc. 113*, 1237–1245.

Bertini, I., Capozzi, F., Ciurli, S., Luchinat, C., Messori, L., & Piccioli, M. (1992a) *J. Am. Chem. Soc. 114*, 3332–3340.

Bertini, I., Capozzi, F., Luchinat, C., Piccioli, M., & Vicens Oliver, M. (1992b) *Inorg. Chim. Acta 198–200*, 483–491.

Bertini, I., Luchinat, C., Ming, L. J., Piccioli, M., Sola, M., & Valentine, J. S. (1992c) *Inorg. Chem. 31*, 4433–4435.

Bertini, I., Campos, A. P., Luchinat, C., & Teixeira, M. (1993a) *J. Inorg. Biochem.* (in press).

Bertini, I., Capozzi, F., Luchinat, C., & Piccioli, M. (1993b) *Eur. J. Biochem. 212*, 69–78.

Blondin, G., Borsch, S. A., & Girerd, J.-J. (1992) *Comments Inorg. Chem. 12*, 315–340.

Blondin, G., & Girerd, J.-J. (1990) *Chem. Rev. 90*, 1359.

Carter, C. W. J., Kraut, J., Freer, S. T., & Alden, R. A. (1974) *J. Biol. Chem. 249*, 6339.

Cowan, J. A., & Sola, M. (1990) *Biochemistry 29*, 5633.

de Ropp, J. S., & La Mar, G. N. (1991) *J. Am. Chem. Soc. 113*, 4348–4350.

Dickson, D. P. E., Johnson, C. E., Cammack, R., Evans, M. C. W., Hall, D. O., & Kao, K. K. (1974) *Biochem. J. 139*, 105.

Dunham, W. R., Hagen, W. R., Fee, J. A., Sands, R. H., Dunbar, J. B., & Humblet, C. (1991) *Biochim. Biophys. Acta 1079*, 253.

Holz, R. C., Que, L., Jr., & Ming, L. J. (1992) *J. Am. Chem. Soc. 114*, 4434–4436.

Johnson, R. D., Ramaprasad, S., & La Mar, G. N. (1983) *J. Am. Chem. Soc. 105*, 7205–7206.

Krishnamoorthi, R., Markley, J. L., Cusanovich, M. A., Przysiecki, C. T., & Meyer, T. E. (1986) *Biochemistry 25*, 60–67.

Kusche, W. H., & Truper, H. G. (1984) *Arch. Microbiol. 137*, 266–271.

Lecomte, J. T. J., Unger, S. W., & La Mar, G. N. (1991) *J. Magn. Reson. 94*, 112–122.

Macura, S., & Ernst, R. R. (1980) *Mol. Phys. 41*, 95.

Middleton, P., Dickson, D. P. E., Johnson, C. E., & Rush, J. D. (1980) *Eur. J. Biochem. 104*, 289–296.

Mouesca, J. M., Lamotte, B., & Rius, G. J. (1991) *Inorg. Biochem. 43*, 251.

Munck, E., Papaefthymiou, V., Surerus, K. K., & Girerd, J.-J. (1988) in *Metal Clusters in Proteins* (Que, L., Jr., Ed.) pp 302, American Chemical Society, Washington, D.C.

Nettesheim, D. G., Meyer, T. E., Feinberg, B. A., & Otvos, J. D. (1983) *J. Biol. Chem. 258*, 8235–8239.

Nettesheim, D. G., Harder, S. R., Feinberg, B. A., & Otvos, J. D. (1992) *Biochemistry 31*, 1234–1244.

Noodleman, L. (1988) *Inorg. Chem. 27*, 3677–3679.

Przysiecki, C. T., Meyer, T. E., & Cusanovich, M. A. (1985) *Biochemistry 24*, 2542.

Rius, G. J., & Lamotte, B. (1989) *J. Am. Chem. Soc. 111*, 2462–2469.

Thauer, R. K., & Schoenheit, P. (1982) in *Iron–Sulfur Proteins* (Spiro, T. G., Ed.) pp 329, Wiley-Interscience, New York.

Thompson, A. J. (1985) in *Metalloproteins* (Harrison, P., Ed.) pp 79, Verlag Chemie, Weinheim, FRG.

Vold, R. L., Waugh, J. S., Klein, M. P., & Phelps, D. E. (1968) *J. Chem. Phys. 48*, 3831–3832.